

See discussions, stats, and author profiles for this publication at: <https://www.researchgate.net/publication/262698492>

Behavior of Lamellar Forming Block Copolymers under Nanoconfinement: Implications for Topography Directed Self-Assembly of Sub-10 nm Structures

ARTICLE *in* MACROMOLECULES · DECEMBER 2013

Impact Factor: 5.8 · DOI: 10.1021/ma4019735

CITATIONS

8

READS

27

8 AUTHORS, INCLUDING:



[Han-Hao Cheng](#)

University of Queensland

23 PUBLICATIONS 105 CITATIONS

[SEE PROFILE](#)



[Michael J. Leeson](#)

Intel

43 PUBLICATIONS 436 CITATIONS

[SEE PROFILE](#)



[Andrew K. Whittaker](#)

University of Queensland

250 PUBLICATIONS 2,808 CITATIONS

[SEE PROFILE](#)



[Idriss Blakey](#)

University of Queensland

98 PUBLICATIONS 882 CITATIONS

[SEE PROFILE](#)

Behavior of Lamellar Forming Block Copolymers under Nanoconfinement: Implications for Topography Directed Self-Assembly of Sub-10 nm Structures

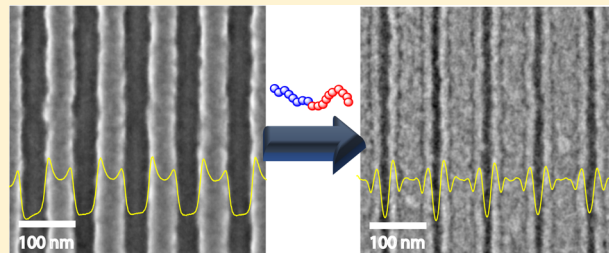
Imelda Keen,^{†,‡} Han-Hao Cheng,[‡] Anguang Yu,^{†,‡} Kevin S. Jack,[§] Todd R. Younkin,^{||} Michael J. Leeson,^{||} Andrew K. Whittaker,^{†,‡} and Idriss Blakey*,^{†,‡}

[†]Australian Institute of Bioengineering and Nanotechnology, [‡]Centre for Advanced Imaging, and [§]Centre for Microscopy and Microanalysis, The University of Queensland, Brisbane, St. Lucia QLD 4072, Australia

^{||}Intel Corporation, Hillsboro, Oregon 97124, United States

S Supporting Information

ABSTRACT: Directed self-assembly of block copolymers (BCPs) is a promising technique for the nanofabrication of structures with dimensions smaller than what can be achieved by current photolithography approaches. In particular, there has been significant interest in the development of BCPs that can achieve ever smaller feature sizes with low levels of defects. Here we investigate the directed self-assembly of a high- χ BCP, polystyrene-block-poly(DL-lactide), which is capable of producing structures with dimensions less than 10 nm. In addition, we study the behavior of the BCP under nanoconfinement and the ability of the polymer chains to compress and stretch in response to the geometry of the confining volume. Key findings of this study are that the level of defects in the self-assembled structures are strongly related to the relative interfacial interactions of the BCP as well as the degree of frustration of the polymer chains under nanoconfinement relative to the bulk. These results have particular significance for nanofabrication of ordered structures, which is of relevance for the fabrication of nanowires, metamaterials, and next-generation computer chips.



INTRODUCTION

Block copolymers (BCPs) consist of at least two chemically distinct polymer chains that are covalently linked. In the bulk, they are capable of phase separating into a range of morphologies with nanoscale dimensions.¹ Favorable physical properties, which are derived from the nanostructure, have led to commercial applications in, for example, adhesives, sealants, and coatings.² On the other hand, there have been a number of investigations that exploit the nanoscale structure of BCPs for fabrication of membranes,³ nanostructured ceramics,⁴ nanowires,⁵ metamaterials,⁶ and photonic materials.⁷

By controlling interfacial interactions of BCPs, it is possible to dictate the orientation of the phase-separated domains in thin films with respect to the substrate.^{8–18} This fundamental advance has enabled the development of directed self-assembly (DSA) of block copolymers, such that patterns generated by top-down lithography are used to control the lateral orientation and/or placement of the phase-separated domains.¹⁹ Depending on the degree of polymerization, the size of the phase-separated domains can be much smaller than features that are able to be printed by optical lithography. This concept allows the creation of templates with densely patterned arrays, which are attractive for a number of nanotechnology-based applications, including pattern multiplication,^{20,21} magnetic-

storage media,^{22,23} healing of lithographic features,²⁴ formation of nanowires,²⁵ and shrinking/repair of contact holes.^{21,26}

DSA can be divided into two categories, namely, graphoepitaxy and chemoepitaxy.¹⁹ Chemoepitaxy uses underlying chemical patterns to guide the self-assembly of BCPs,²⁷ where, for example, one of the surface chemistries interacts preferentially with one of the blocks. In contrast, graphoepitaxy uses topographical patterns, such as patterns etched into inorganic substrates,^{28–33} or patterned photoresists,^{21,34–36} to guide the self-assembly. In both these scenarios, when the size of the guiding template is comparable, but incommensurate with the natural long period of the bulk BCP (L_0), the morphology of the confined BCP may differ significantly compared with the bulk morphology. For example, this phenomenon was initially studied in thin films confined between two planar substrates. It was found that the domains of lamella-forming polystyrene-block-poly(methyl methacrylate) (PS-*b*-PMMA) that were oriented parallel to the substrate could stretch or compress to be commensurate with the confining width.^{37–39}

Received: September 24, 2013

Revised: October 24, 2013

Published: December 26, 2013

Cheng and co-workers were the first to investigate the behavior of BCPs confined in patterned templates. Specifically, they investigated the behavior of polystyrene-*b*-poly(ferrocenyldimethylsilane), with a bulk spherical morphology, that was confined in trenches with widths that corresponded to varying degrees of commensurability.^{31,33} They observed that the number of rows formed within the trenches were quantized but that the row spacing varied for different trench widths to accommodate an integer number of spherical structures. A significant finding was that the spacing of the rows was smaller near the walls of the trenches due to the presence of a wetting layer. Xiao et al.³⁰ studied the behavior of PS-*b*-PMMA with a cylindrical morphology confined within trenches, in which the surface chemistry of the sidewalls and substrate had been modified to have no preferential interactions with the BCP. In this case, the domains were also found to deform, but the row spacing was found to be uniform across the entire trench due to the presence of a nonpreferential surface chemistry on the sidewalls. Another consequence of the nonpreferential surface chemistry was that partial cylindrical domains were pinned to the sidewalls. Recently, Xu et al.⁴⁰ investigated cylinder-forming PS-*b*-poly(ethylene oxide) (PEO) confined by underlying chemical templates rather than topography. They demonstrated that compression and stretching of the domains were also observed for chemoepitaxy. Such findings are of great significance for applications in bit-patterned media and integrated circuit manufacture because nanometer precision in the placement of features is required.

In this article we study the behavior of a series of lamella-forming polystyrene-*b*-poly(DL-lactide) (PS-*b*-PLA) confined in narrow trenches. PS-*b*-PLA, which was first reported by Zalusky and co-workers,⁴¹ has a high Flory–Huggins polymer–polymer interaction parameter ($\chi = 0.217$ at 298 K⁴¹) and hence is capable of achieving much smaller feature sizes than the widely studied PS-*b*-PMMA. Unlike some other high- χ BCPs, PS-*b*-PLA also has the advantage of being compatible with thermal annealing, making processing simpler. However, in a similar fashion to PS-*b*-PMMA there is a choice of using the surface chemistry of the substrate^{17,42} or solvent vapor⁴² to orient the phase-separated domains perpendicular to the substrate. Hillmyer's group^{43,44} has used thin films with oriented domains to fabricated nanostructured membranes and nanodot arrays for next generation hard drives. Here we demonstrate that it was possible to perform graphoepitaxy-based DSA of PS-*b*-PLA using a standard extreme ultraviolet (EUV) lithography resist as a template, such that ordered sub-10 nm lines and spaces could be achieved. In addition, we investigated the effect of the confinement volume and commensurability on the levels of defects in the self-assembled structures. The findings have implications for implementation of high- χ BCPs for high-resolution graphoepitaxy DSA.

EXPERIMENTAL METHODS

Materials. Triphenylsulfonium triflate, ethyl lactate, styrene, DL-lactide, copper(I) bromide, styrene, trioctylamine, N,N,N',N'',N''-pentamethyldiethylenetriamine (PMDETA), and 1,8-diazabicyclo[5.4.0]undec-7-ene (DBU) were obtained from Sigma-Aldrich. 4-Hydroxybutyl 2-bromoisobutyrate was prepared using the method described by Yang and co-workers.⁴⁵ 350 kDa PMMA was obtained from PolySciences Inc. E²Stack AL412 was obtained from Brewer Science. (Poly[(4-hydroxystyrene)_{0.6}-co-(styrene)_{0.2}-co-(tert-butyl acrylate)_{0.2}]), 38 wt %, in ethyl lactate (trade name JSR 622HSB-EL), was obtained from JSR Corp. The synthesis of a series of symmetrical PS-*b*-PLA block copolymers (14.7, 15.9, 21, and 28

kDa) as well as 22 kDa PS and 13 kDa PLA homopolymers have been described previously.^{17,46} Briefly, they were prepared by first polymerizing styrene using atom transfer radical polymerization (ATRP),^{55,56} using copper(I) bromide and PMDETA as the catalyst system.^{47,48} The initiator for ATRP had a hydroxyl group (4-hydroxybutyl 2-bromoisobutyrate), so the polystyrene had hydroxyl end functionality at the α -chain end. The polystyrene macroinitiator was chain extended with DL-lactide using organo-catalyzed ring-opening polymerization (ROP) via the hydroxyl end-group.⁴⁹ Molecular weight parameters of the BCPs are shown in Table S1.

Preparation of EUV Patterned Resists. A proprietary polymer solution, E²Stack AL412, was spun onto silicon wafers to form a thin film, a so-called “assist layer”, with a thickness of about 20 nm. Following this an EUV-sensitive, positive tone photoresist (4.76 wt % poly[(4-hydroxystyrene)_{0.6}-co-(styrene)_{0.2}-co-(tert-butyl acrylate)_{0.2}], 0.44 wt % triphenylsulfonium triflate, and 0.076 wt % trioctylamine in ethyl lactate) was spin-coated onto the wafers, which was followed by annealing at 105 °C on a hot plate for 1 min to give a film with a thickness of 55 nm, which was determined by spectroscopic ellipsometry. The wafers were exposed on an EUV microexposure tool (MET).^{50,51} Following exposure the wafers were annealed at 95 °C for 60 s, and then the regions that were exposed to EUV light were removed by rinsing with 2.38% TMAH at room temperature for 30 s, rinsing in deionized water, and drying with a stream of N₂ gas. The result was wafers with 1:1 line-space patterns with trench widths ranging from 22 to 500 nm.

DSA of PS-*b*-PLA Guided by EUV Patterned Resists. Solutions of PS-*b*-PLA (1 wt %, in anisole) with molecular weights of 14.7, 15.9, 21, and 28 kDa were spin-coated onto the EUV patterned wafers and then annealed at 100 °C for 24 h at reduced pressure (600 mmHg). Scanning electron microscopy images were obtained using a field emission scanning electron microscope (SEM) (Raith-150, Raith, GmbH), using a secondary in-lens detector with an accelerating voltage of 2 kV and working distance of 3 mm.

Etch Selectivity of PS-*b*-PLA Block Copolymers. Solutions of 22 kDa PS, 350 kDa PMMA, and 13 kDa PLA in propylene glycol methyl ether acetate (2 wt %) were spin-coated onto silicon wafers. Following spin-coating the coated wafers were annealed on a hot plate in air at 140 °C for 5 min. The film thicknesses were measured using a vacuum UV-variable-angle spectroscopic ellipsometer (J.A. Woollam Co.). Ar and O₂ plasma etching was carried out in a customized system at 20 W, for 30 s, at a pressure of 30 mTorr, which was achieved by using a gas flow rate of 5 sccm. The thicknesses of the remaining films was measured using ellipsometry. The etch selectivities presented here were calculated with respect to PS.

Contact Angle Measurements. Thin films of various polymers were prepared by spin-coating 2 wt % solutions from PGMEA. A mimic of the patterned photoresist sidewalls was prepared using a bilayer method described by Prahbu et al.⁵² using specific parameters previously reported by Chuang and co-workers.²⁴ Static contact angles were measured using a Data Physics Instruments Optical Contact Angle Series 5 (OCA 5) goniometer. The contact angles reported here were measured by the addition of a 5 μ L drop of either water or diiodomethane at five different locations for each thin film.

RESULTS AND DISCUSSION

The Graphoepitaxy Process. Figure 1 shows a schematic detailing the process used in this study for the directed self-assembly of PS-*b*-PLA. First EUV lithography was used to pattern a multilayer film that consisted of a commercially available polymeric underlayer and an open-source EUV photoresist formulation as the top layer (70 nm) (Figure 1*i,ii*). This process yielded line-space patterns, where the widths of the trench ranged from 43.8 to 108 nm. These templates were then spin-coated with solutions of PS-*b*-PLA in anisole (Figure 1*iii*). To induce ordering of the BCPs, the wafers were then annealed (Figure 1*iv*), and selective removal of the PLA blocks was facilitated by plasma etching (Figure 1*v*).

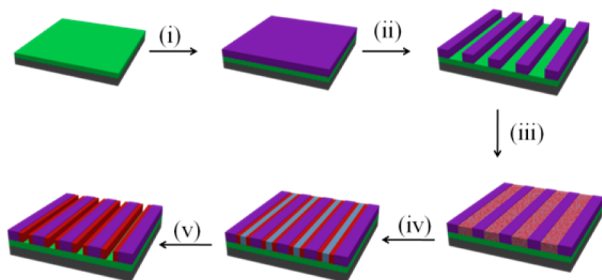


Figure 1. Workflow for graphoepitaxy-based directed self-assembly of PS-*b*-PLA: (i) deposition of EUV photoresist (purple) on Si wafer (gray) coated with a polymer-based under-layer (green); (ii) patterning of resist using EUVL; (iii) spin-coating of PS-*b*-PLA; (iv) thermal annealing to induce phase separation of the PS (red) and PLA (light blue) blocks; (v) selective etching of PLA via plasma etching.

Morphology of PLA-*b*-PS in the Trenches. Figure 2 shows top-down SEM micrographs of three sequential steps, where Figure 2a was after EUVL patterning of the photoresist, Figure 2b was after directed self-assembly of 21 kDa PS-*b*-PLA in the trenches, and Figure 2c was after the wafer underwent reactive ion etching. The yellow profiles in each image represent the average pixel intensity in the vertical direction. To allow easy comparison, the micrographs have been aligned so that repeating lithographic patterns line up down the images. In Figure 2a, the bright regions (i) correspond to the remaining resist polymer and the dark regions (ii) to trenches where the resist has been removed by developer. The average width of the trenches (W_T) was measured to be 43.8 ± 0.6 nm, which for the 21 kDa PS-*b*-PLA corresponds to $2.06L_0$.

After DSA of the 21 kDa PS-*b*-PLA was performed (Figure 2b), the remaining resist has an intermediate contrast (iii). Within any given trench two bands of bright intensity (iv) can be observed as well as three bands of lower pixel intensity: one in the center of the trench with the lowest intensity (v) and two narrower bands at the edge of the trench, which have intensities in between the resist and the central low intensity band (vi). The original width of the trench was equivalent to $2.06L_0$ of the BCP, so a probable configuration is three full domains ($0.5L_0$) and two half domains ($0.25L_0$) serving as a wetting layer at the walls of the trenches. In these experiments the BCPs were confined in trenches consisting of three solid interfaces, which include the underlayer coating and the two side walls of the trench, the latter being comprised of the photoresist polymer, as well as being unconstrained at the polymer–air interface. The interfacial energies (γ) of each block with the side walls ($\gamma_{\text{PLA-wall}}$, $\gamma_{\text{PS-wall}}$) and the underlayer ($\gamma_{\text{PLA-UL}}$, $\gamma_{\text{PS-UL}}$) should provide an insight into the expected morphologies of the PS-*b*-PLA in the trenches. The two harmonic liquid method⁵³ was used to estimate the respective surface energies at these interfaces, which were then used to calculate the γ values that are listed in Table 1. The low value of $\gamma_{\text{PLA-wall}}$ compared with $\gamma_{\text{PS-wall}}$ indicates that the PLA blocks are expected to preferentially interact with the sidewalls compared with the PS blocks. From these results the most probable configuration of the BCP in the trenches is that PLA blocks form thin wetting layers on the resist sidewalls (vi in Figure 2b), and consequently the bright bands (iv in Figure 2b) are due to PS domains and the low-intensity band in the center of the trenches (v in Figure 2b) are due to PLA domains (see Figure 3). This configuration is consistent with Walton et al.,³⁹ who considered the confinement of thin films of lamella-forming

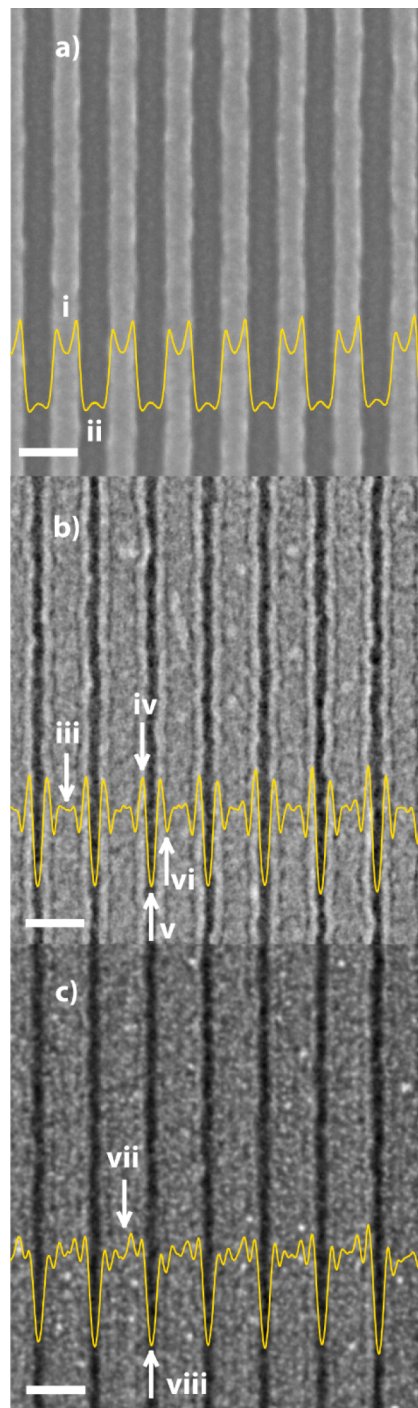


Figure 2. Top-down SEMs illustrating the three stages of the directed self-assembly (DSA) of 21 kDa PS-*b*-PLA in the trenches of lithographic templates. The yellow profiles represent the average pixel intensity in the vertical direction. The scale bars = 100 nm. (a) EUVL patterned resist template: (i) the light contrast corresponds to the remaining resist polymer, (ii) while the dark contrast corresponds to the trenches. (b) After DSA of a 21 kDa PS-*b*-PLA guided by the template: (iii) the brightest contrast corresponds to PS domains, (iv) and (v) the darkest contrast to the PLA domains, and (vi) the intermediate contrast the resist template. (c) After O₂ plasma etching for 30 s: (vii) the dark contrast corresponds to the etched PLA domains and (viii) the lighter contrast to the remaining resist and PS domains.

Table 1. Summary of Interfacial Energies for Each Block at Relevant Interfaces

interface	interfacial energy (mJ m^{-2})
$\gamma_{\text{PLA-wall}}$	0.1
$\gamma_{\text{PS-wall}}$	5.3
$\gamma_{\text{PLA-UL}}$	0.4
$\gamma_{\text{PS-UL}}$	4.6
$\gamma_{\text{PLA-PS}}$	4.3

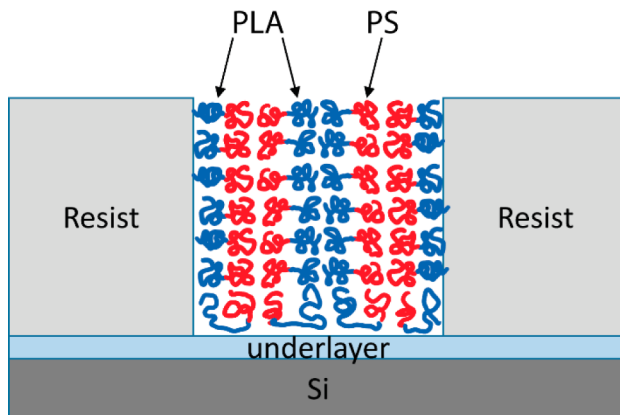


Figure 3. Schematic showing the configuration of the block copolymers within a trench with a width of approximately $2L_0$.

BCPs between two hard interfaces, with identical surface chemistries. For example, when one block preferentially interacts with both of the hard interfaces, orientation of the lamellae parallel to the interfaces is typically favored. Furthermore, the domain widths adjacent to the hard interface should be half the thickness of domains in the center of the film, such that the total number of long periods observed is an integer.

To further confirm the identity of the different phases, the wafers were subjected to plasma etching, which using appropriate conditions can selectively remove one of the polymers. To determine these conditions, the O_2 plasma etch rates were determined for each of the homopolymers which were found to be 1.8 nm/min for PS, 5.4 nm/min for PLA, and 1.8 nm/min for the photoresist. This corresponds to an etch selectivity of about 3:1 for PLA over PS and the photoresist, indicating that the PLA blocks will be selectively etched under these conditions. This was also supported by etching experiments performed on thin films of BCP. For example, Figure S1 shows top-down SEM micrographs of lamellar forming PS-*b*-PLA that have their domains oriented perpendicular to the substrate, before and after etching. It can be seen that after etching the contrast increases significantly due to loss

of one of the blocks. Figure S2 then shows the SEM micrographs of the etched sample which has been tilted to 45° , and it is apparent that one of the blocks has been preferentially removed. The high-resolution XPS traces of the C 1s region in Figure S3 then show that there is greater loss of the C=O and C–O bands which are associated with the PLA blocks compared to the C–C band which is associated with both the PS and PLA. This confirms that the PLA blocks are being preferentially removed during etching. If the etched DSA sample is now considered (Figure 2c), the brighter bands (vii) are attributed to the remaining polymer, which from the etch rates above will be the PS and the photoresist. The band of lower intensity in the center of each trench can then be attributed to regions where the PLA has been etched. These results confirm the configuration proposed in Figure 3. The fact that the wetting layer is not clearly observed by SEM is probably due to two reasons: (1) the secondary electron emission is affected by charging which limits the contrast at high resolution, and (2) the roughness of the lines of photoresist was on the order of 5 nm when measured to 3σ , which is comparable to the domain size of the wetting layer.

Behavior of PS-*b*-PLA under Nanoconfinement. To investigate the effect of the confining width on the morphology of the BCP following DSA, 21 kDa PS-*b*-PLA BCPs was deposited into trenches with widths of 43.8, 44.3, 46.1, 60.7, and 71 nm. The top-down SEM images are shown in Figure 4a–e. For Figure 4a–c the trench widths correspond to $2.06–2.16L_0$, and two long periods can be observed in each image. The 60.7 nm trenches (Figure 4d) correspond to $2.85L_0$, and while domains can be observed near the walls of the trench, the morphology is not clear in the center of the trench. Increasing the width of the trench to 71 nm, which corresponds to $3.73L_0$, results in three long periods being observed. From these experiments it can be seen that to a certain extent the lamellar domains of the BCP are capable of stretching to be commensurate with W_T .

The behavior of the 14.7, 15.9, and 28 kDa PS-*b*-PLA BCPs in same templates was also studied. The results for all of the BCPs have been summarized in Figure 5 as a function of the normalized confinement width (W_T/L_0). Figure 5a shows the number of long periods (n) confined in the trenches. Equation 1 was used to estimate the degree of compression, or stretching of the domains (λ) and this is shown in Figure 5b.

$$\lambda = W_T/nL_0 \quad (1)$$

It can be seen that for the series of BCPs tested the domains were capable of being compressed or stretched relative to the bulk domains (Figure 5b). Furthermore, a crossover (n to $n + 1$) was observed to occur at $W_T \sim L_0(n + \frac{1}{2})$. This observation was consistent with small-angle neutron reflectivity measurements of symmetrical PS-*b*-PMMA^{37,38,54,55} and poly(ethylene-

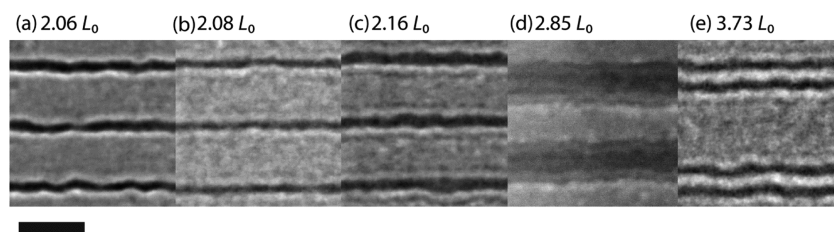


Figure 4. Directed self-assembly of a 21 kDa PS-*b*-PLA within trenches for a range of widths (a) $2.06L_0$, 43.8 ± 0.6 nm; (b) $2.08L_0$, 44.3 ± 0.5 nm; (c) $2.16L_0$, 46.1 ± 0.5 nm; (d) $2.85L_0$, 60.7 ± 0.4 nm; and (e) $3.73L_0$, 79.4 ± 0.4 nm. Scale bar = 100 nm.

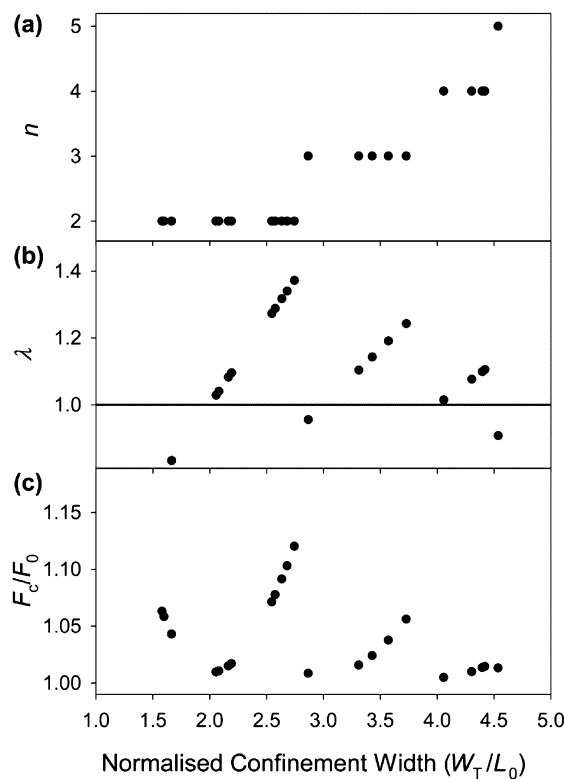


Figure 5. Variation of the physical parameters for the BCP as a function of the dimensionless confinement width. (a) Number of long periods observed. (b) Degree of domain stretching or compression (λ). (c) Variation of the free energy of the confined chains relative to that of the bulk (F_C/F_0).

co-propylene)-*b*-poly(ethylene)⁵⁶ BCPs confined as thin films between two planar substrates, in which lamellae were oriented parallel to the substrate. Analogous behavior has also been reported for the graphoepitaxy of sphere^{33,57} and cylinder-forming³⁰ BCPs as well as for chemoepitaxy of cylindrical domains.⁴⁰ However, to the best of our knowledge,

this is the first detailed investigation of nanoconfinement effects for lamella-forming systems undergoing directed self-assembly.

The free energy of the confined chains (F_C) relative to the free energy of the bulk configuration (F_0) has also been calculated for each sample using eqs 2 and 3, which were originally developed by Turner et al.⁵⁸ for thin films of lamella confined between two identical planar substrates, where one block has preferential interactions with the confining walls:

$$\frac{F_C}{F_0} = \frac{1}{3} \left(\lambda^2 + \frac{2}{\lambda} + \frac{2\Gamma}{n\lambda} \right) \quad (2)$$

where

$$\Gamma = \frac{\gamma_{\text{PLA-wall}}}{\gamma_{\text{PLA-PS}}} \quad (3)$$

and $\gamma_{\text{PLA-wall}}$ and $\gamma_{\text{PLA-PS}}$ were taken from Table 1. The resulting values of F_C/F_0 have been plotted as a function of the confinement width (Figure 5c). From comparison of the plots in Figure 5 it can be seen that that the free energy of the confined chain relative to the bulk increases up until just above $W_T = L_0(n + \frac{1}{2})$, where a transition from n to $n + 1$ occurs and the relative free energy drops to a minimum at $W_T \sim nL_0$. This demonstrates that the maximum frustration of the conformation of the BCP chains occurs at around $W_T = L_0(n + \frac{1}{2})$ and is consistent with the behavior that has previously been observed for sphere^{33,57} and cylinder-forming^{30,40} systems undergoing directed self-assembly.

Long-Range Ordering and Levels of Defects. To demonstrate the effect of commensurability on the long-range order and level of defects of the self-assembled structures, lower resolution SEM micrographs of the DSA of 21 kDa PS-*b*-PLA ($L_0 = 21.3$ nm, by SAXS¹⁷) were acquired (Figure 6a,b). The average trench width for Figure 6a was $2.08L_0$, and it can be seen that the morphology is relatively consistent across the images, while for Figure 6b, $W_T = 2.85L_0$ and defects in the lamella morphology begin to appear (e.g., blue arrows), particularly where the roughness of the sidewalls effectively increases the localized width of the trench. A slightly different

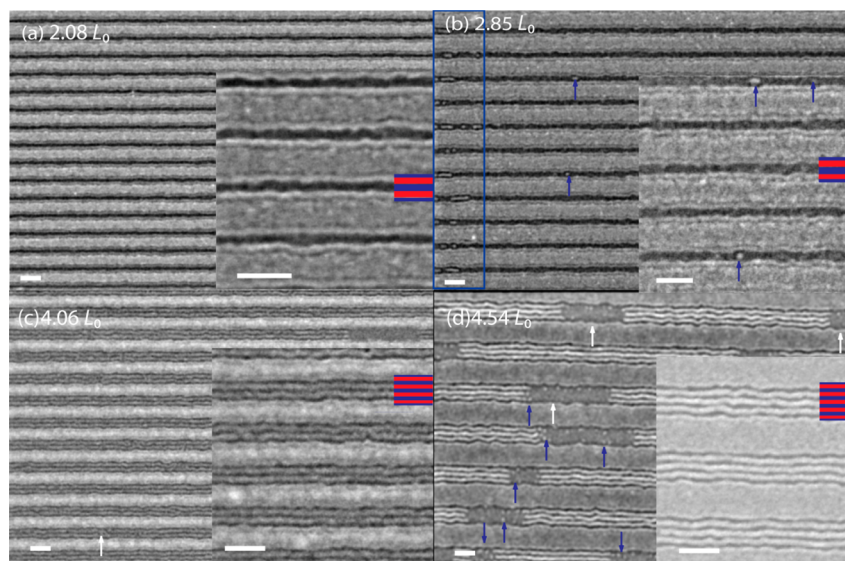


Figure 6. Top-down SEM images with high-resolution insets of the DSA of 21 kDa PS-*b*-PLA in trenches with widths of (a) $2.08L_0$ and (b) $2.85L_0$. DSA of 14.7 kDa PS-*b*-PLA in trenches with widths of (c) $4.06L_0$ and (d) $4.54L_0$. The colored schematic insets show the suggested conformation of the lamellae in the resist template, such that the PLA domains are represented by blue and the PS domains by red. The scale bars = 100 nm.

situation was observed for the DSA of 14.7 kDa PS-*b*-PLA ($L_0 = 17.5$ nm, by SAXS¹⁷) in trenches with widths of $4.06L_0$ (Figure 6c) and $4.54L_0$ (Figure 6d), where four (~9 nm domains) and five long periods (~8 nm domains) were observed, respectively. When the width of the trench was $4.06L_0$, some defects could be observed (e.g., indicated by white arrows), but the long-range ordering was significantly better compared with the $4.54L_0$ trenches for which numerous defects were observed. For example, with the $4.54L_0$ trenches there were regions where no morphology was obvious (white arrows) and other regions where an apparently cylindrical morphology was observed (blue arrows).

At least two factors contribute to the levels of defects in these systems. The first involves a combination of conformational frustration (F_C/F_0) and the roughness of the sidewalls. In this scenario the relative free energy of the chains compared to the bulk will be high when $W_T \sim L_0(n + 1/2)$, and because the roughness of the sidewalls is significant relative to the domain size, a mixture of n and $n + 1$ domains can be observed, such as in Figure 6b. On the other hand, when $W_T \sim nL_0$, the stretching and compression of the domains can compensate for the roughness of the sidewalls and the level of defects are low (e.g., Figure 6a). For the EUVL printed lines in this study the 3σ deviation of the actual line edge from an ideal, straight line edge was in the order of 5 nm, which is typical for EUVL resist patterns. The 21 kDa PS-*b*-PLA has an L_0 of 21.3 nm, which corresponds to a domain size of 10.6 nm, with the smallest natural domain size in this study being 8.7 nm. From comparing the line edge roughness with domain size, it can be seen that for high- χ BCPs, such as PS-*b*-PLA, the domain size is approaching the roughness of the lithographically printed lines. While the stretching and compression can accommodate this roughness for a range of widths (e.g., Figure 6a), when the polymer chains have a high degree of frustration (e.g., Figure 6b), where $W_T = 2.85L_0$, the morphology was no longer uniform; hence, with many research groups investigating higher- χ BCPs, these problems will require consideration.

A second factor that contributes to the level of defects involves the relative contribution of the interaction of the PLA with the sidewalls compared with the interaction of PLA with the underlayer. The results in Table 1 indicate that the underlayer is not expected to be a neutral surface for PS-*b*-PLA, such that the PLA blocks are expected to interact preferentially compared with the PS block. When W_T was small, the contributions of the sidewall interactions dominated, but progressively decrease with increasing W_T . For example, the ratio of interfacial areas of the sidewalls and underlayer were 3.2, 2.3, 2, and 1.8 for Figure 6a–d, respectively. In Figure 6a, the long-range order was good, but in Figure 6c defects in the morphology were observed despite the good commensurability of L_0 with W_T . In Figure 6d, it can be seen that the frequency of defects was much higher, and the regions with no apparent structure were likely due to the lamellar domains adopting a configuration that was parallel to the substrate due to the interactions of the BCP with the underlayer beginning to dominate over the interactions with the sidewalls. The significance of these findings is that when the interactions of the block copolymer with the photoresist side walls dominate the interactions of the block copolymer with the substrate, it may not be necessary for the surface chemistry of the base of the trench to have nonpreferential interactions with the BCPs; i.e., a neutral surface is not necessarily required. For the BCP systems studied in this work, such a condition is met when the

width of the trench is of the order of $2L_0$. However, for wider trenches, particularly when the conformation of the polymer chains was highly frustrated, significant numbers of defects can be observed. This should be able to be overcome by using an underlayer with nonpreferential interactions with each of the blocks in PS-*b*-PLA; however, the strict requirements regarding metal impurities for the EUVL tool that was used precluded the use of neutral underlayers that we had previously developed.⁵⁹

A potential concern when relying on top-down SEM or AFM micrographs to gauge the morphology of a confined system is that the results may not be entirely representative of the underlying morphology. For example, simulations have shown that for certain conditions the morphology observed at the surface can be drastically different to the underlying morphology.⁶⁰ Using small-angle X-ray scattering, Perera and co-workers⁶¹ have shown that lamellar domains can undergo subtle deformation of domain shape. Similarly, Wang et al. observed distortions in the morphology of triblock copolymers using resonant soft X-ray scattering and transmission electron microscopy tomography. However, the geometry of the samples in this study was not compatible with these analysis techniques. Another approach to test this is to perform a selective etch of one of the blocks followed by top-down SEM analysis. In this study O₂ plasma etching was used to selectively etch the PLA block.

Figure 7 shows a SEM image after DSA of 21 kDa PS-*b*-PLA in 108 nm trenches and a 30 s O₂ plasma exposure. The overall

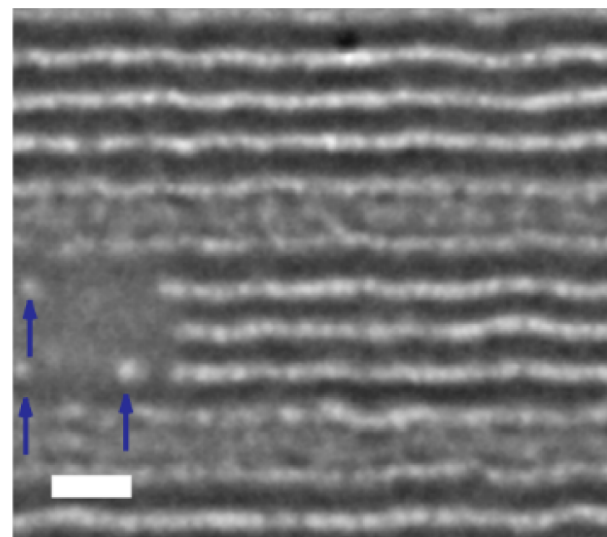


Figure 7. SEM micrographs showing the residual PS domains after O₂ plasma of (a) 21 kDa PS-*b*-PLA within 46 nm (the scale bar = 50 nm) and (b) 108 nm trenches. The blue arrows point to areas where cylindrical morphology was observed (scale bar = 100 nm).

morphology of the etched samples was consistent with prior to etching (Figure 6d); i.e., a lamellar morphology can be seen before and after etching. In addition, some of the cylindrical defects can be observed in Figure 7, which were also observed in the sample prior to etching. These results suggest that the morphology observed at the surface persists throughout the film but does not rule out a PLA wetting layer being present at the substrate. Indeed, some distortion of the morphology may be evident. For example, it is apparent that the width of the newly formed trenches where the PLA has been etched were slightly wider, with an average width of approximately 14 nm

from 11 nm, while the remaining PS domains are slightly thinner with widths of ca. 9 nm from 11 nm. This is consistent with the underlying substrate having preferential interactions with the PLA block. For example, simulations of lamella-forming PS-*b*-PMMA on substrates with differing affinities for the two blocks revealed that the block with the strongest interaction with the substrate tended to become wider at the substrate–polymer interface compared with the polymer–air interface, while the block with the weaker interaction tended to be narrower closer to the substrate–polymer interface.⁶⁰ However, it is also possible that the etching process was not 100% anisotropic and the apparent decrease in width of the remaining PS domains may be due to etching of the PS domains.

Discussion of the Benefits of PS-*b*-PLA for DSA. The properties of PS-*b*-PLA endow it with a number of advantages in performance and ease of processing. In particular, the high- χ parameter (0.217 at 298 K) leads to performance advantages because much smaller features can be assembled compared to PS-*b*-PMMA ($\chi = 0.05$). For example, lines as thin as 8.7 nm were printed. In addition, similar to PS-*b*-PMMA, PS and PLA have similar surface energies (38.2 \pm 0.3 and 45.0 \pm 0.2 mJ/m², respectively), and the consequence of this is that the orientation of lamellar morphologies perpendicular to a substrate can be accessed when appropriate neutral interfaces are used, which has not been reported for high- χ silicone-based block copolymers.

Other key parameters include a low annealing temperature to induce phase separation (100 °C), which was significantly lower than the T_g of the resist polymer (123 °C) and the spin-coating solvent was a poor solvent for the photoresist, causing minimal resist deformation (Supporting Information, Figures S4 and S5). Therefore, radiation cross-linking^{36,61,62} or chemical “freezing”⁶³ of the photoresist polymer template was not required. For example, directed self-assembly of PS-*b*-PMMA using a photoresist template typically requires annealing temperatures in excess of 180 °C,²¹ and therefore in those cases an additional step involving cross-linking or treatment of the patterned resist with a chemical “freezing” agent has been required, which can lead to an undesirable change in the dimensions of the patterned features.⁶² Hence, elimination of the “freezing” step was a key processing advantage. The fact that PS-*b*-PLA was compatible with thermal annealing is also significant because many other high- χ BCPs require solvent annealing, which is difficult to integrate into a manufacturing process.

CONCLUSIONS

The directed self-assembly of a high- χ BCP, PS-*b*-PLA, to give phase-separated lamellar domains aligned parallel to the resist template and perpendicular to the substrate was demonstrated. Domain sizes as small as 8.7 nm were achieved. The annealing temperature to induce phase separation was below the T_g of the photoresist, and the spin-coating solvent used was a poor solvent for the photoresist, so no freezing or cross-linking step was required, which is often the case for other systems. The strong interaction of the trench sidewalls with the PLA block has directed the lamellar domains to be orientated perpendicular to the substrate and parallel to the lithographic patterns, despite an underlayer that had preferential interactions with the PLA block being used. Confined lamellar domains were found to compress and contract to be commensurate with the width of the trenches of

the patterned photoresist, and it was found that the numbers of defects in our BCP systems increased with increasing width of trenches, particularly when the degree of conformational frustration was high compared to the bulk. The findings of this study highlight the potential of PS-*b*-PLA to be used in the nanofabrication of ordered linear structures with sublithographic dimensions.

ASSOCIATED CONTENT

S Supporting Information

Supplementary SEM images. This material is available free of charge via the Internet at <http://pubs.acs.org>.

AUTHOR INFORMATION

Corresponding Author

*E-mail: i.blakey@uq.edu.au (I.B.).

Notes

The authors declare no competing financial interest.

ACKNOWLEDGMENTS

This research was supported under the Australian Research Council (ARC) Linkage Projects Scheme (project number LP0989607) and by Intel Corporation. I.B. and A.K.W. also acknowledge the ARC for a Future Fellowship (FT100100721) and Australian Professorial Fellowship (DP100104299), respectively. Experiments were carried out in part at the Centre for Microscopy and Microanalysis (CMM), The University of Queensland (UQ); Queensland node of the Australian Microscopy and Microanalysis Research Facility, UQ; and the Australian National Fabrication Facility (ANFF) (UQ and Australian National University nodes (ANU)). The authors also thank Drs. Barry Wood (CMM) and Gordon Xu (ANNF-ANU) for their assistance in conducting experiments.

REFERENCES

- (1) Ruzette, A.-V.; Leibler, L. *Nat. Mater.* **2005**, *4*, 19–31.
- (2) Holden, G. Thermoplastic Elastomers. In *Applied Plastics Engineering Handbook*; Myer, K., Ed.; William Andrew Publishing: Oxford, 2011; pp 77–91.
- (3) Jackson, E. A.; Hillmyer, M. A. *ACS Nano* **2010**, *4*, 3548–3553.
- (4) Malenfant, P. R. L.; Wan, J.; Taylor, S. T.; Manoharan, M. *Nat. Nanotechnol.* **2007**, *2*, 43–46.
- (5) Thurn-Albrecht, T.; Schotter, J.; Kästle, G. A.; Emley, N.; Shibauchi, T.; Krusin-Elbaum, L.; Guarini, K.; Black, C. T.; Tuominen, M. T.; Russell, T. P. *Science* **2000**, *290*, 2126–2129.
- (6) Vignolini, S.; Yu, N. A.; Cunha, P. S.; Guldin, S.; Rushkin, I.; Stefk, M.; Hur, K.; Wiesner, U.; Baumberg, J. J.; Steiner, U. *Adv. Mater.* **2012**, *24*, OP23–OP27.
- (7) Schacher, F. H.; Rupar, P. A.; Manners, I. *Angew. Chem., Int. Ed.* **2012**, *51*, 7898–7921.
- (8) Mansky, P.; Liu, Y.; Huang, E.; Russell, T. P.; Hawker, C. *Science* **1997**, *275*, 1458–1460.
- (9) Sohn, B. H.; Yun, S. H. *Polymer* **2002**, *43*, 2507–2512.
- (10) Han, E.; In, I.; Park, S. M.; La, Y. H.; Wang, Y.; Nealey, P. F.; Gopalan, P. *Adv. Mater.* **2007**, *19*, 4448–4452.
- (11) Han, E.; Stuen, K. O.; La, Y.-H.; Nealey, P. F.; Gopalan, P. *Macromolecules* **2008**, *41*, 9090–9097.
- (12) Ji, S.; Liu, C.-C.; Son, J. G.; Gotrik, K.; Craig, G. S. W.; Gopalan, P.; Himpel, F. J.; Char, K.; Nealey, P. F. *Macromolecules* **2008**, *41*, 9098–9103.
- (13) Han, E.; Stuen, K. O.; Leolukman, M.; Liu, C.-C.; Nealey, P. F.; Gopalan, P. *Macromolecules* **2009**, *42*, 4896–4901.
- (14) Ryu, D. Y.; Ham, S.; Kim, E.; Jeong, U.; Hawker, C. J.; Russell, T. P. *Macromolecules* **2009**, *42*, 4902–4906.

- (15) Bates, C. M.; Strahan, J. R.; Santos, L. J.; Mueller, B. K.; Bamgbade, B. O.; Lee, J. A.; Katzenstein, J. M.; Ellison, C. J.; Willson, C. G. *Langmuir* **2011**, *27*, 2000–2006.
- (16) Liu, H.; O'Mahony, C. T.; Audouin, F.; Ventura, C.; Morris, M.; Heise, A. *Macromol. Chem. Phys.* **2012**, *213*, 108–115.
- (17) Keen, I.; Yu, A.; Cheng, H.-H.; Jack, K. S.; Nicholson, T. M.; Whittaker, A. K.; Blakey, I. *Langmuir* **2012**, *28*, 15876–15888.
- (18) Bates, C. M.; Seshimo, T.; Maher, M. J.; Durand, W. J.; Cushen, J. D.; Dean, L. M.; Blachut, G.; Ellison, C. J.; Willson, C. G. *Science* **2012**, *338*, 775–779.
- (19) Cheng, J. Y.; Pitera, J.; Park, O.-H.; Flickner, M.; Ruiz, R.; Black, C. T.; Kim, H.-C. *Appl. Phys. Lett.* **2007**, *91*, 143106.
- (20) Ruiz, R.; Ruiz, N.; Robert, Y. Z.; Sandstrom, L.; Black, C. T. *Adv. Mater.* **2007**, *19*, 2157–2162.
- (21) Cheng, J. Y.; Sanders, D. P.; Truong, H. D.; Harrer, S.; Friz, A.; Holmes, S.; Colburn, M.; Hinsberg, W. D. *ACS Nano* **2010**, *4*, 4815–4823.
- (22) Ruiz, R.; Dobisz, E.; Albrecht, T. R. *ACS Nano* **2010**, *5*, 79–84.
- (23) Park, S.; Lee, D. H.; Xu, J.; Kim, B.; Hong, S. W.; Jeong, U.; Xu, T.; Russell, T. P. *Science* **2009**, *323*, 1030–1033.
- (24) Chuang, Y.-M.; Jack, K. S.; Cheng, H. H.; Whittaker, A. K.; Blakey, I. *Adv. Funct. Mater.* **2013**, *23*, 173–183.
- (25) Gowd, E. B.; Nandan, B.; Vyas, M. K.; Bigall, N. C.; Eychmüller, A.; Schlörb, H.; Stamm, M. *Nanotechnology* **2009**, *20*, 415302.
- (26) Yi, H.; Bao, X.-Y.; Zhang, J.; Bencher, C.; Chang, L.-W.; Chen, X.; Tiborio, R.; Conway, J.; Dai, H.; Chen, Y.; Mitra, S.; Wong, H. S. P. *Adv. Mater.* **2012**, *24*, 3107–3114.
- (27) Cheng, J. Y.; Rettner, C. T.; Sanders, D. P.; Kim, H.-C.; Hinsberg, W. D. *Adv. Mater.* **2008**, *20*, 3155–3158.
- (28) Segalman, R. A.; Yokoyama, H.; Kramer, E. J. *Adv. Mater.* **2001**, *13*, 1152–1155.
- (29) Sundrani, D.; Darling, S. B.; Sibener, S. J. *Langmuir* **2004**, *20*, 5091–5099.
- (30) Xiao, S. G.; Yang, X. M.; Edwards, E. W.; La, Y. H.; Nealey, P. F. *Nanotechnology* **2005**, *16*, S324–S329.
- (31) Cheng, J. Y.; Ross, C. A.; Thomas, E. L.; Smith, H. I.; Vancso, G. J. *Adv. Mater.* **2003**, *15*, 1599–1602.
- (32) Park, S.-M.; Rettner, C. T.; Pitera, J. W.; Kim, H.-C. *Macromolecules* **2009**, *42*, 5895–5899.
- (33) Cheng, J. Y.; Mayes, A. M.; Ross, C. A. *Nat. Mater.* **2004**, *3*, 823–828.
- (34) Ilievski, F.; Ross, C. A. *J. Vac. Sci. Technol., B* **2010**, *28*, 42–44.
- (35) Jeong, S.-J.; Kim, J. E.; Moon, H.-S.; Kim, B. H.; Kim, S. M.; Kim, J. B.; Kim, S. O. *Nano Lett.* **2009**, *9*, 2300–5.
- (36) Cheng, H.-H.; Keen, I.; Yu, A.; Chuang, Y.-M.; Blakey, I.; Jack, K. S.; Leeson, M. J.; Younkin, T. R.; Whittaker, A. K. *Proc. SPIE* **2011**, *7970*, 79701V.
- (37) Kellogg, G. J.; Walton, D. G.; Mayes, A. M.; Lambooy, P.; Russell, T. P.; Gallagher, P. D.; Satija, S. K. *Phys. Rev. Lett.* **1996**, *76*, 2503–2506.
- (38) Lambooy, P.; Russell, T. P.; Kellogg, G. J.; Mayes, A. M.; Gallagher, P. D.; Satija, S. K. *Phys. Rev. Lett.* **1994**, *72*, 2899–2902.
- (39) Walton, D. G.; Kellogg, G. J.; Mayes, A. M.; Lambooy, P.; Russell, T. P. *Macromolecules* **1994**, *27*, 6225–6228.
- (40) Xu, J.; Russell, T. P.; Checco, A. *Small* **2013**, *9*, 779–784.
- (41) Zalusky, A. S.; Olayo-Valles, R.; Wolf, J. H.; Hillmyer, M. A. *J. Am. Chem. Soc.* **2002**, *124*, 12761–12773.
- (42) Vayer, M.; Hillmyer, M. A.; Dirany, M.; Thevenin, G.; Erre, R.; Sinturel, C. *Thin Solid Films* **2010**, *518*, 3710–3715.
- (43) Phillip, W. A.; O'Neill, B.; Rodwgin, M.; Hillmyer, M. A.; Cussler, E. L. *ACS Appl. Mater. Interfaces* **2010**, *2*, 847–853.
- (44) Baruth, A.; Rodwgin, M. D.; Shankar, A.; Erickson, M. J.; Hillmyer, M. A.; Leighton, C. *ACS Appl. Mater. Interfaces* **2011**, *3*, 3472–3481.
- (45) Chang, S. W.; Ayothi, R.; Bratton, D.; Yang, D.; Felix, N.; Cao, H. B.; Deng, H.; Ober, C. K. *J. Mater. Chem.* **2006**, *16*, 1470–1474.
- (46) Blakey, I.; Yu, A.; Howdle, S. M.; Whittaker, A. K.; Thurecht, K. J. *Green Chem.* **2011**, *13*, 2032–2037.
- (47) Matyjaszewski, K.; Xia, J. *Chem. Rev.* **2001**, *101*, 2921–2990.
- (48) Peng, H.; Blakey, I.; Dargaville, B.; Rasoul, F.; Rose, S.; Whittaker, A. K. *Biomacromolecules* **2009**, *10*, 374–381.
- (49) Dove, A. P.; Pratt, R. C.; Lohmeijer, B. G. G.; Culkin, D. A.; Hagberg, E. C.; Nyce, G. W.; Waymouth, R. M.; Hedrick, J. L. *Polymer* **2006**, *47*, 4018–4025.
- (50) Roberts, J. M.; Bacuita, T.; Bristol, R. L.; Cao, H. B.; Chandhok, M.; Lee, S. H.; Panning, E. M.; Shell, M.; Zhang, G.; Rice, B. J. *Proc. SPIE* **2005**, *5751*, 64–77.
- (51) Caudillo, R.; Younkin, T.; Putna, S.; Myers, A.; Shroff, Y.; Bacuita, T.; Kloster, G.; Sohmen, E. *Proc. SPIE* **2010**, *7636*, 76363I.
- (52) Prabhu, V. M.; Kang, S.; VanderHart, D. L.; Satija, S. K.; Lin, E. K.; Wu, W.-L. *Adv. Mater.* **2010**, *388*–408.
- (53) Owens, D. K.; Wendt, R. C. *J. Appl. Polym. Sci.* **1969**, *13*, 1741–1747.
- (54) Russell, T. P.; Lambooy, P.; Kellogg, G. J.; Mayes, A. M. *Physica B: Condens. Matter* **1995**, *213*–214, 22–25.
- (55) Park, S. M.; Stoykovich, M. P.; Ruiz, R.; Zhang, Y.; Black, C. T.; Nealey, P. F. *Adv. Mater.* **2007**, *19*, 607–611.
- (56) Koneripalli, N.; Singh, N.; Levicky, R.; Bates, F. S.; Gallagher, P. D.; Satija, S. K. *Macromolecules* **1995**, *28*, 2897–2904.
- (57) Cheng, J. Y.; Zhang, F.; Chuang, V. P.; Mayes, A. M.; Ross, C. A. *Nano Lett.* **2006**, *6*, 2099–2103.
- (58) Turner, M. S. *Phys. Rev. Lett.* **1992**, *69*, 1788–1791.
- (59) Keen, I.; Yu, A.; Cheng, H.-H.; Jack, K. S.; Nicholson, T.; Whittaker, A. K.; Blakey, I. *Langmuir* **2012**, *28*, 15876–15888.
- (60) Detcheverry, F. A.; Pike, D. Q.; Nealey, P. F.; Muller, M.; de Pablo, J. J. *Faraday Discuss.* **2010**, *144*, 111–125.
- (61) Perera, G. M.; Wang, C.; Doxastakis, M.; Kline, R. J.; Wu, W.-L.; Bosse, A. W.; Stein, G. E. *ACS Macro Lett.* **2012**, *1*, 1244–1248.
- (62) Wallow, T. I.; Rayasam, M.; Yamaguchi, M.; Yamada, Y.; Kim, R.-H.; Kye, J.; Levinson, H. J. *J. Micro-Nanolith. MEM* **2009**, *8*, 011010–011010.
- (63) Bae, Y. C.; Liu, Y.; Cardolaccia, T.; McDermott, J. C.; Trefonas, P.; Spizuoco, K.; Reilly, M.; Pikon, A.; Joesten, L.; Zhang, G. G.; Barclay, G. G.; Simon, J.; Gaurigan, S. *Proc. SPIE* **2009**, *7273*, 727306.